Dynamic and Earthquake Behaviour of Greek Post-Byzantine Churches with Foundation Deformability—Experimental Investigation of Stone Masonry Material Properties

George C. Manos, Lambros Kotoulas, Vasiliki Matsou and Olympia Felekidou

Abstract The dynamic and earthquake behaviour of Post-Byzantine Christian churches made of stone masonry is examined. All these churches developed damage to their masonry elements due to the amplitude of the gravitational and seismic actions combined with the deformability of the foundation. The numerical results together with assumed strength values are utilized to predict the behaviour of the various masonry parts in in-plane, shear, and normal stress as well as out-of-plane flexure. It is shown that the foundation deformability partly explains the appearance of structural damage. When comparing the numerically predicted regions that reach limit state conditions with actual damage patterns a reasonably good agreement in a qualitative sense can be observed. The masonry walls near the foundation, the door and window openings and the roof appear to be the most vulnerable either in out-of-plane bending or in in-plane shear for the critical combination of seismic forces and gravitational loads. The vaults and domes of the superstructure also appear to be vulnerable. The effectiveness of retrofitting schemes is also discussed. A relatively mild retrofitting scheme is examined that utilizes special mortar injections as well as semi-temporary shoring together with wooden and metal ties. The numerical investigation is supplemented with a series of limited laboratory tests on constituent materials which represent old stone masonry.

Keywords Post-Byzantine churches · Numerical simulation · Deformable foundation · Experimental study of stone masonry properties · Retrofitting

---

G.C. Manos (✉) · L. Kotoulas · V. Matsou · O. Felekidou
Laboratory of Strength of Materials and Structures, Department of Civil Engineering, Aristotle University of Thessaloniki, Thessaloniki, Greece
e-mail: gcmanos@civil.auth.gr

I.N. Psycharis et al. (eds.), *Seismic Assessment, Behavior and Retrofit of Heritage Buildings and Monuments*, Computational Methods in Applied Sciences 37, DOI 10.1007/978-3-319-16130-3_9

1 Introduction

During the last 30 years various parts of Greece have been subjected to a number of damaging earthquakes ranging from Ms = 5.2 to Ms = 7.2 on the Richter scale. One of the most demanding tasks for counteracting the consequences of all these seismic events was the effort to ensure the structural integrity of old churches, which were built from 400 A.D. onwards. In many cases they sustained considerable damage [1]. The earthquake behaviour of Christian churches belonging to the so-called Post-Byzantine period (16th to 19th century A.D.) has been studied numerically in some detail [2–8]. In all these cases the foundation was considered to be non-deformable. However, this is a gross approximation as in most cases these churches are founded on deformable soil. In some instances, the deformability of the soil caused considerable damage as is the case of the church of The Assumption of Virgin Mary at Dilofo-Voio-Kozani as presented in Sect. 2. In some other cases the main cause of recent damage is the earthquake activity that is exacerbated by the deformability of the soil. This is the case for the damaged churches of Agia Triada at Vithos-Kozani and of Profits Elias at Siatista-Kozani that are also presented. Finally, a summary of retrofitting principles together with brief results from a relevant numerical and experimental investigation focusing on the behaviour of St. Dimitrios of Palatitsia is also presented. It is interesting to note that all these churches were built in a number of phases on old existing sacred sites by extending old remains. This was due to prohibitions by the Turkish occupation authorities imposed on the Christian population not to construct new churches but only to maintain existing ones.

2 The Assumption of Virgin Mary at Dilofo-Voio-Kozani

The outlay of this church is shown in Fig. 1, by a cross-section in the longitudinal direction; its basic dimensions are 21.5 m long (together with the apse of the East wall), 11 m wide and a maximum height to the top of the wooden roof 10 m. The soft soil is indicated with the dashed line. As can be seen, the West part of this

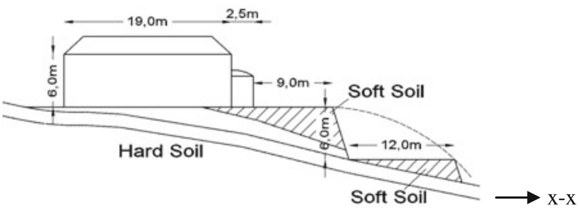

Fig. 1 The layout of the church of Virgin Mary

church is founded on hard soil (weathered flysch layers) whereas the East part is founded on relatively soft soil that was deposited on top of the layers to compensate for the natural slope at this location. Apart from the relatively soft soil deposits at the East part of this church the malfunction of the drainage system at this part initiated considerable settlement of these soft soil deposits.

The unequal settlement of the foundation of the stone masonry walls as well as of the internal columns that supported the vaulting system that covered this church caused considerable damage. An external view of this church from the South is shown in Fig. 2a whereas Fig. 2b depicts the extensive damage that developed at the South-East corner. A very wide crack initiates at the top of the East external wall near the apse and propagates towards the bottom of this wall being inclined to the South-East corner. A similarly wide crack propagates through the North external wall from top to bottom as is shown in Fig. 2c. It must be noted that the thickness of these masonry walls varies from 750 to 800 mm. From this extensive peripheral wall damage the vaulting system that is supported by these peripheral walls also suffered extensive cracking that eventually caused the partial collapse of a part of the central dome, as shown in Fig. 2d.

Fig. 2 Damage of the church of the assumption of Virgin Mary at Dilofo-Voio-Kozani. **a** View from the South (August 2010). **b** View from the South-East (August 2010). **c** View from the South (August 2010). **d** Partial collapse of the central dome (2011)

2.1 Numerical Simulation of the Seismic Behaviour

Initially, the numerical simulation assumed that the foundation was non-deformable [9]. Based on this assumption the 3-D numerical representation of the church, including the peripheral walls, the vaulting system of the superstructure, as shown in Fig. 3, and the wooden roof were subjected to load combinations either 0.9G±1.4Ex or 0.9G±1.4Ey, where G is the gravitational load and Ex, Ey the earthquake forces [10] along the x-x axis (longitudinal East-West direction) or the y-y axis (transverse North-South direction), respectively.

All the supports were assumed to prohibit the translations along all three axes but not to restrain the rotations. It was found from previous studies that full fixity of the supports leads to the development of considerable bending moments that correspond to tensile stresses that cannot be sustained by the weak stone masonry used to construct these churches. For the load combination 0.9G+1.4(+Ex) the maximum deformations at the top of the central dome were found equal to Ux = 6.81 mm Uz = −1.51 mm (Fig. 3). For this load combination the maximum tensile stresses parallel to the bed joint were found equal to 0.38 and 0.51 MPa, at the top face and bottom face of the masonry walls, respectively (Fig. 4). As can be seen in this figure, high tensile stresses parallel to the bed joint develop both at the top of the North wall and at the South-East corner of the East wall.

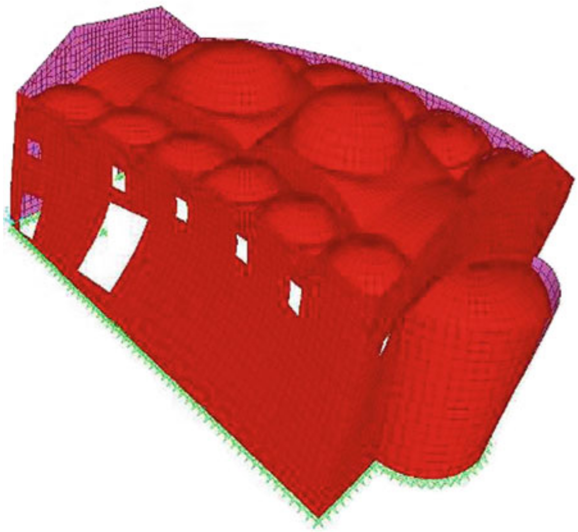

Fig. 3 Non-deformable soil for the load combination 0.9G +1.4(+Ex). G = the gravitational forces, Ex = the earthquake forces. Displacement response at: the top of central dome
Ux = 6.81 mm
Uz = −1.51 mm

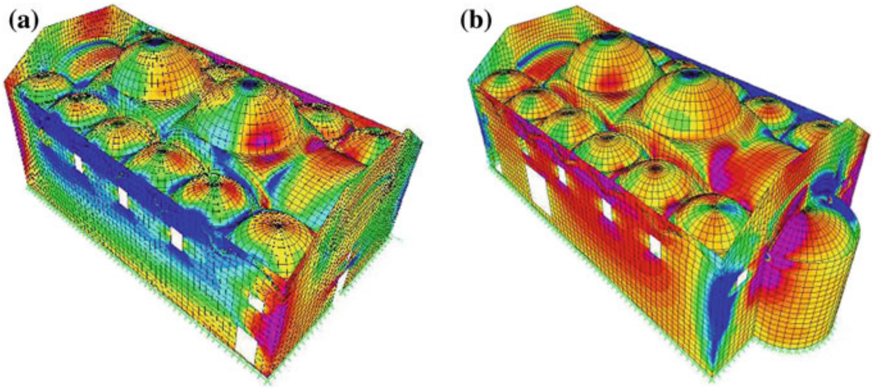

Fig. 4 Non-deformable soil. Load combination 0.9G+1.4(+Ex), out-of-plane stress response, **a** $\boldsymbol{\sigma}_{11}$ *top face*, max$\boldsymbol{\sigma}$ = 0.38 MPa, **b** $\boldsymbol{\sigma}_{11}$ *bottom face*, max$\boldsymbol{\sigma}$ = 0.51 MPa

2.1.1 Numerical Simulation of the State of Stress Arising from the Foundation Settlement

Next, layers of deformable soil were introduced beneath the foundation of all the peripheral walls and internal colonnades (Fig. 5). The stiffness of these soil layers was varied in order to simulate the relatively hard soil at the West part of the church and the relatively soft soil at the North-East part of the church (see Fig. 1). For quantifying the stiffness of these soil layers, use was made of the data from three boreholes drilled in the vicinity of the church to ascertain the constitution of the soil deposits at a depth up to 10 m [9]. For the load combination 0.9G+1.4(+Ex), the maximum deformations at the top of the central dome were found equal to Ux = 21.33 mm Uz = −14.80 mm; these values represent a considerable increase of the deformations at the top of the church from the previous case where the soil was considered non-deformable (see Figs. 3 and 5).

Figure 6 depicts the distribution of stresses $\boldsymbol{\sigma}_{11}$ parallel to the bed joint; the maximum tensile values were found equal to 0.53 and 0.64 MPa at the top and bottom face of the masonry walls, respectively (Fig. 6). As can also be seen in this figure, high tensile stresses parallel to the bed joint develop both at the top of the North wall and at the South-East corner of the East wall. The increase in the tensile stresses for the deformable soil is of the order of 30–50 % when compared to the corresponding maximum tensile stresses if the soil were to be considered non-deformable. As could be seen from the preceding numerical study, the uneven deformability of the soil under the foundation of such structural formations as the Post-Byzantine Basilicas can introduce an increase in the critical tensile stresses. The regions of such tensile stress concentration correlates reasonably well with the locations of damage that was actually observed in this church.

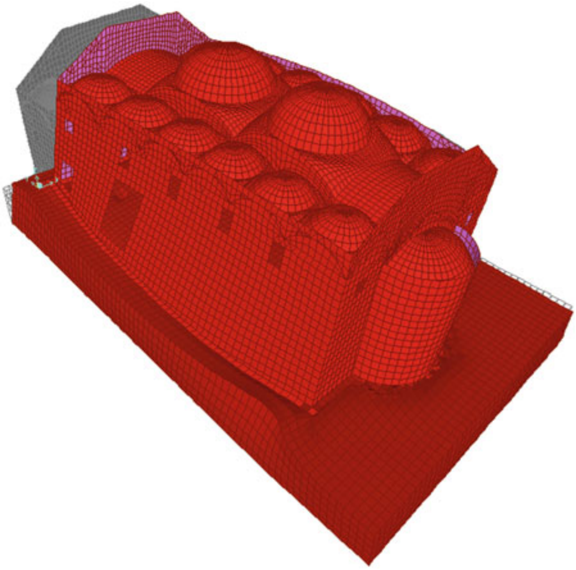

Fig. 5 Deformable soil for the load combination 0.9G+1.4(+Ex). G = the gravitational forces, Ex = the earthquake forces. Displacement response at: the top of central dome Ux = 21.33 mm Uz = −14.80 mm

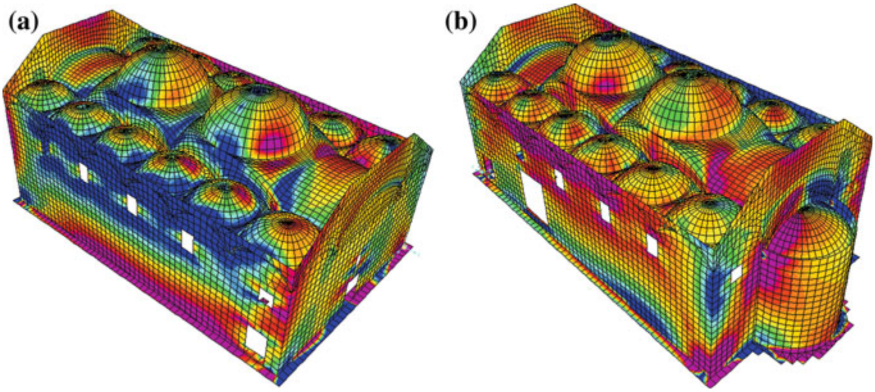

Fig. 6 Out-of-plane behaviour, deformable soil. Load combination 0.9G+1.4(+Ex), **a** $\boldsymbol{\sigma_{11}}$ *top face*, max$\boldsymbol{\sigma}$ = 0.53 MPa, **b** $\boldsymbol{\sigma_{11}}$ *bottom face*, max$\boldsymbol{\sigma}$ = 0.64 MPa

3 The Holy Trinity (Agia Triada) at Vithos-Voio-Kozani

This is a Post-Byzantine church of the cruciform with three domes typology. The central dome rises at the highest elevation to 15.75 m from the ground level; the length of the church in the longitudinal East-West direction is 17.60 m and its width

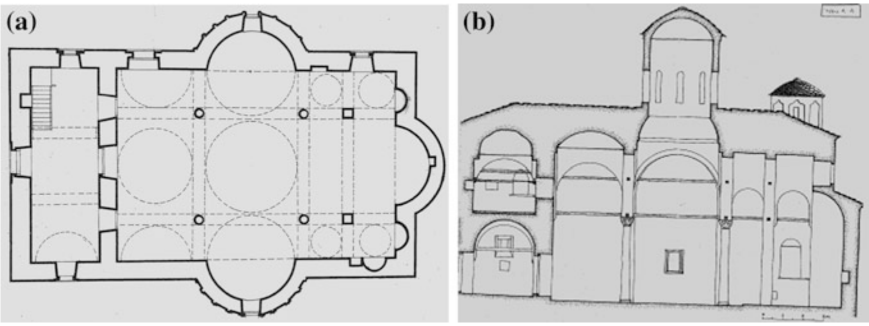

Fig. 7 The church of Holy Trinity (Agia Triada) at Vithos-Voio-Kozani. **a** Plan. **b** East-West section, view from South

in the North-South direction is 9.85 m. The construction of this stone-masonry church was completed in 1797 A.D. using the local natural stone.

The plan and the East-West cross-section are shown in Fig. 7a, b. The vaulting system that supports the three domes is depicted in Fig. 8c, d, as can be seen from the top by removing the wooden roof (Fig. 8a, b). The numerical simulation considered two distinct models. The first model was assumed to be supported on a non-deformable foundation where the translations along the three axes (x, y, z) were restrained to be equal to zero.

The second model attempts to account for the deformability of the foundation by using as supports linear springs with stiffness properties that were estimated taking into consideration the quality of the underlying media (Fig. 9) as well as the thickness of the foundation and the discretization employed.

The modal analysis results, shown in Figs. 10 and 11, demonstrate the effect of the deformable foundation which is the lengthening of the eigen-periods of the most significant translational modes.

In addition, we see the mobilization of larger modal mass ratios for these eigenmodes when the foundation was considered deformable than the corresponding values of the modal mass ratios for the non-deformable foundation. Next, the deformations of the structural system were obtained for both the non-deformable and the deformable foundation model. These were obtained for two sets of load combination; one that is designated as 0.9G+1.4Ex and signifies the combination of the gravitational forces (G) with the seismic actions in the East-West (x-x) longitudinal direction. The response from the seismic action was obtained from the application of the dynamic spectral method with a design spectrum specified by the current Greek Seismic Code and for seismic Zone I and soil category A [10]. The second load combination is designated as 0.9G+1.4Ey and denotes the combination of the gravitational forces (G) with the seismic actions in the North-South (y-y) transverse direction. Summary results are depicted in Fig. 12a–d. The load combinations 0.9G±1.4Ex or 0.9G±1.4Ey are used instead of the G±Ex±0.3Ey or G ±0.3Ex±Ey, specified by the codes, as indirect way two combine the two horizontal

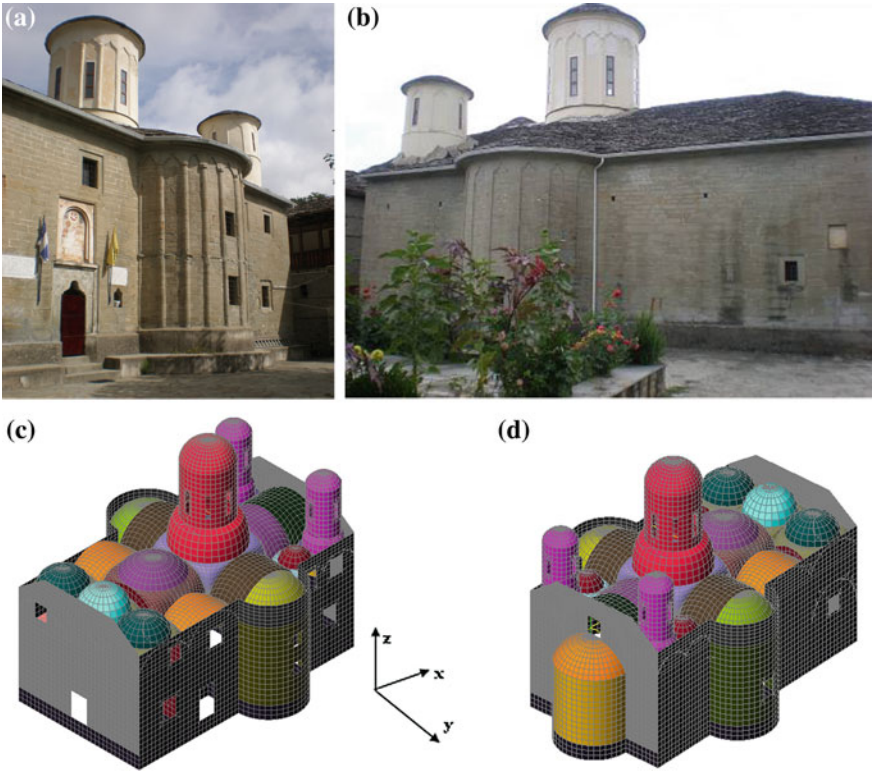

Fig. 8 The church of Holy Trinity (Agia Triada) at Vithos-Voio-Kozani. **a** Side view from the South. **b** Damage of the central dome. **c** View from the South-West. **d** View from the North-East

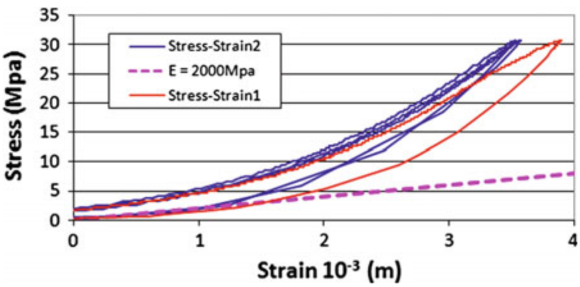

Fig. 9 Compressive stress-strain behaviour of a slate sample taken from the vicinity of the church

components of the seismic action bearing in mind that the masonry piers are checked separately for the in-plane and out-of-plane state of stress. Moreover, gravity forces increase the strength of unreinforced masonry against shear; their reduction (through the multiplier 0.9) is a realistic precaution.

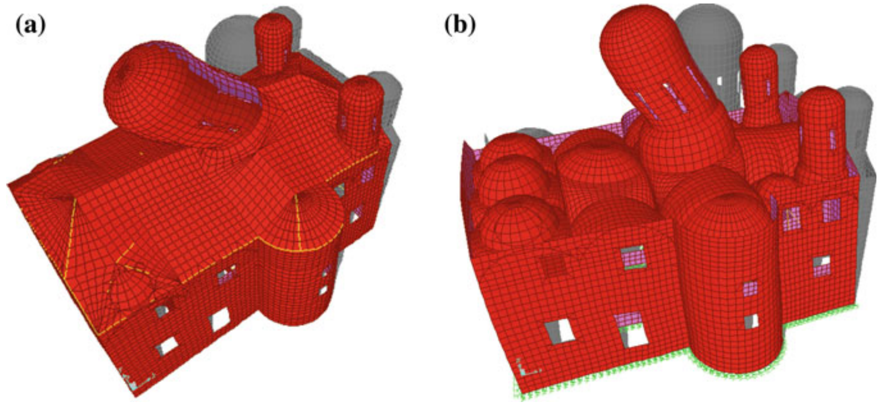

Fig. 10 1st translational eigen-mode y-y. **a** Non-deformable foundation Ty = 0.154 s modal mass ratio Uy = 44.67 %. **b** Deformable foundation Ty = 0.197 s modal mass ratio Uy = 60.26 %

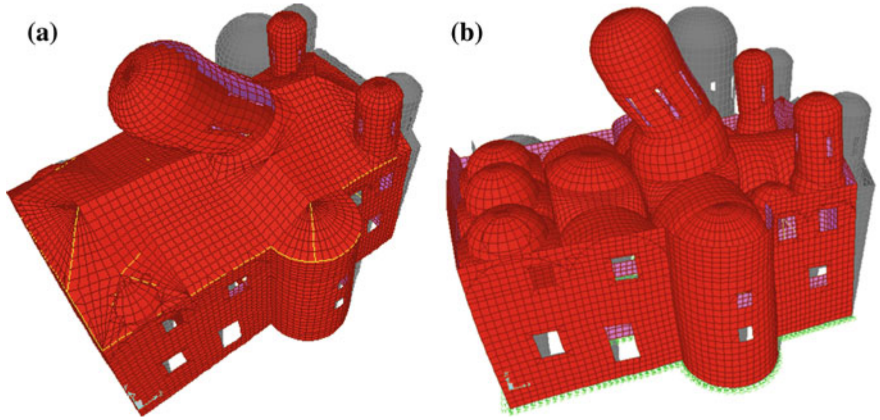

Fig. 11 2nd translational eigen-mode x-x. **a** Non-deformable foundation Tx = 0.135 s. **b** Deformable foundation Tx = 0.159 s modal mass ratio Ux = 61.68 %

Due to the foundation deformability the earthquake actions combined with the gravitational forces result in a considerable increase in the horizontal displacement response. This is more pronounced at the top of the peripheral wall where the vaults of the superstructure and roof are supported than at the top of the central dome level. At that level, the maximum displacement is equal to 14.710 m for the deformable foundation and 13.779 mm for the non-deformable foundation for the load combination 0.9G+1.4Ex. For the load combination 0.9G+1.4Ey the maximum displacement at the top of the central dome level is 13.442 mm for the non-deformable foundation as compared with 14.640 mm for the deformable foundation. Similar influence of the foundation deformability can also be observed

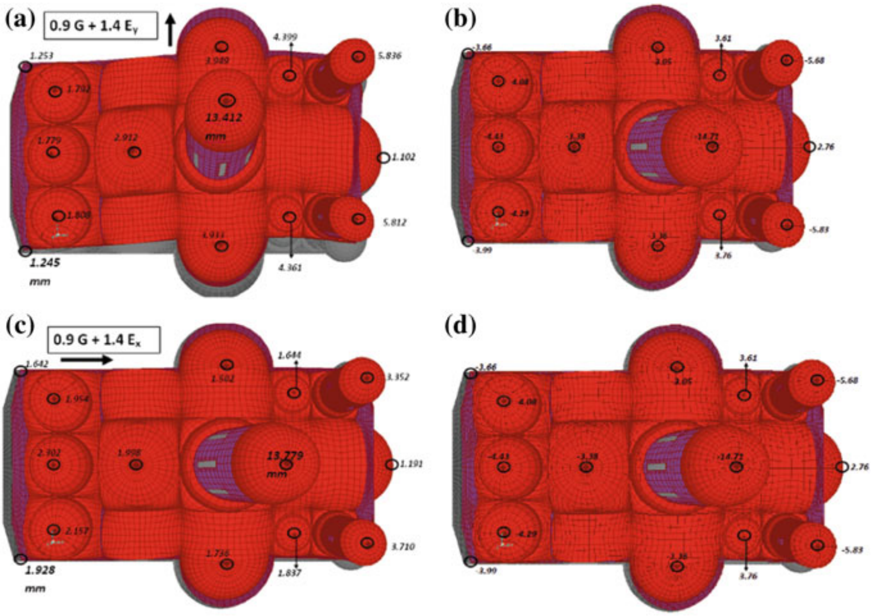

Fig. 12 Maximum displacement response for load combinations 0.9G+1.4E$_y$, 0.9G+1.4E$_x$. **a** Non-deformable foundation Max. Disp. y-y top central dome 13.442 mm. **b** Deformable foundation Max. Disp. y-y top central dome 14.640 mm. **c** Non-deformable foundation Max. Disp. x-x top central dome 13.779 mm. **d** Deformable foundation Max. Disp. x-x top central dome 14.710 mm

in the maximum stress values that develop at either the peripheral walls the internal transverse wall or the vaults of the superstructure.

Figures 13 and 14 depict the tensile stress concentration at the outer (top) face of the vaulting system, as it results from either load combination 0.9G+1.4Ex or 0.9G +1.4Ey. As can be seen from these figures, the foundation deformability increases the tensile stress demand at critical locations for the vaulting of the superstructure. This observation that derives from the numerical results is also supported by in situ evidence of damage to the masonry parts of the vaulting system as shown in Fig. 15.

Figure 16a, b depict the shear stress concentration at the internal transverse wall for the load combination 0.9G+1.4Ey. As can be seen in these figures, the foundation deformability increases the shear stress demand at critical locations at the bottom where the masonry piers are formed between the door and window openings.

Table 1 lists the assumed mechanical characteristics for the stone masonry in terms of Young's modulus and Poisson's ratio as well as compressive and tensile strength values [11].

Moreover, a Mohr-Coulomb failure envelope was adopted, as defined by Eq. 1, for the in-plane shear limit state of the stone masonry, when a normal stress ($\boldsymbol{\sigma_n}$) is acting simultaneously [2–8, 11].

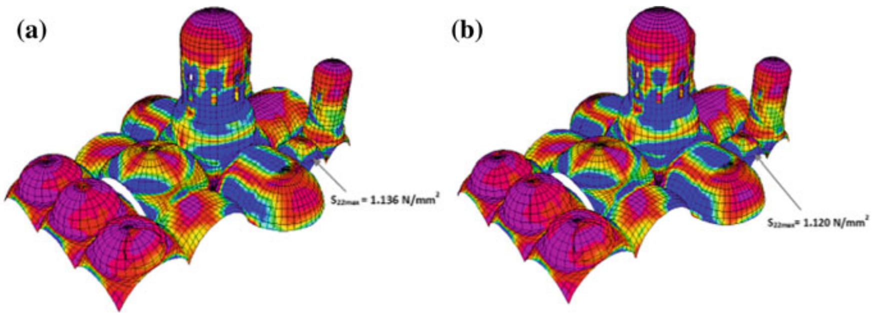

Fig. 13 State of stress for the vaulting system—load combination 0.9G+1.4(+Ey). **a** Non-deformable foundation *top face* Max. Tensile $\boldsymbol{\sigma_{22}}$ 1.136 MPa. **b** Deformable foundation *top face* Max. Tensile $\boldsymbol{\sigma_{22}}$ 1.120 MPa

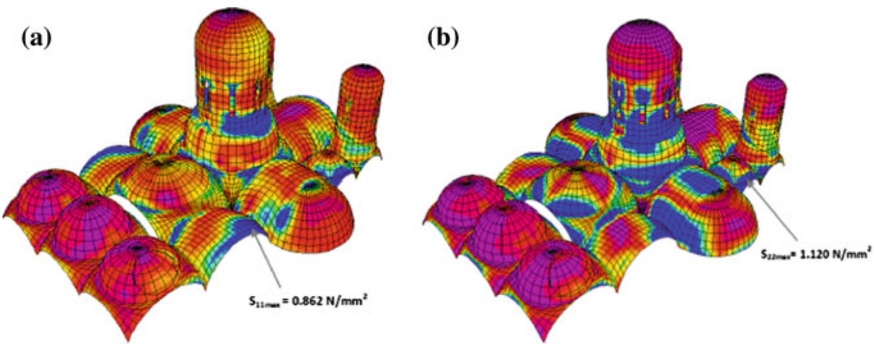

Fig. 14 State of stress for the vaulting system—load combination 0.9G+1.4(+Ex). **a** Non-deformable foundation *top face* Max. Tensile $\boldsymbol{\sigma_{11}}$ 0.862 MPa. **b** Deformable foundation *top face* Max. Tensile $\boldsymbol{\sigma_{11}}$ 0.935 MPa

Fig. 15 Damage of the vaulting system. **a** Central dome. **b** North vaulting. **c** Central arch

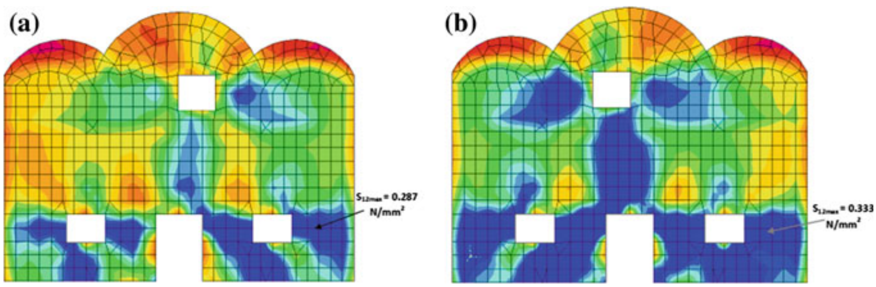

Fig. 16 State of shear stress internal transverse wall—load combination 0.9G+1.4(+Ey). **a** Non-deformable foundation Max in-plane shear stress $\boldsymbol{\tau_{12}}$ 0.287 MPa. **b** Deformable foundation Max in-plane shear stress $\boldsymbol{\tau_{12}}$ 0.333 MPa

Table 1 Assumed mechanical characteristics of the stone masonry

	Young's modulus (N/mm^2)	Poisson's ratio	Compressive strength (N/mm^2)	Tensile Strength normal/parallel bed-joint (N/mm^2)	Initial shear strength f_{vko} (N/mm^2)
Limit values	2500	0.2	3.80	0.250/0.800	0.19

$$\mathbf{f_{vk}} = \mathbf{f_{vko}} + 0.4\,\boldsymbol{\sigma}_\mathbf{n} \tag{1}$$

where: $\mathbf{f_{vko}}$ is the initial shear strength of the stone masonry when the normal stress ($\boldsymbol{\sigma}_\mathbf{n}$) is zero; $\mathbf{f_{vko}}$ was assumed to be equal to 0.192 N/mm^2.

Next, certain commonly used failure criteria, employed for masonry, were adopted for either in-plane tension/compression or shear or out-of-plane tension. All the masonry parts of the studied structure were examined in terms of in-plane and out-of-plane stress demands against the corresponding capacities, as these capacities were obtained by applying the Mohr-Coulomb criterion of Eq. 1 or the stone masonry compressive and tensile strength limits listed in Table 1. Due to space limitations such results are not shown in detail here. Selective results, obtained from this evaluation process, are shown in Figs. 17, 19, 21 and 22. With $\mathbf{R}\boldsymbol{\sigma}$ or with $\mathbf{R}\boldsymbol{\tau}$ the ratios of the in-plane tensile or shear strength value over the corresponding demand are denoted whereas with $\mathbf{R_M}$ the ratio of the out-of-plane tensile strength value over the corresponding demand is denoted. Ratio values smaller than 1.0 indicate that a limit state condition is reached thus predicting structural damage. This approach combines numerical stress demands, resulting from elastic analyses, with limit-state strength values. A different approach is to include these limit-state strength values with a non-linear push-over type of analyses, as was done by Manos et al. [2]. It was shown that the simplified approach applied here correlates quite well in predicting regions of structural damage (Figs. 15, 18, 20) with such a more complex non-linear approach [2].

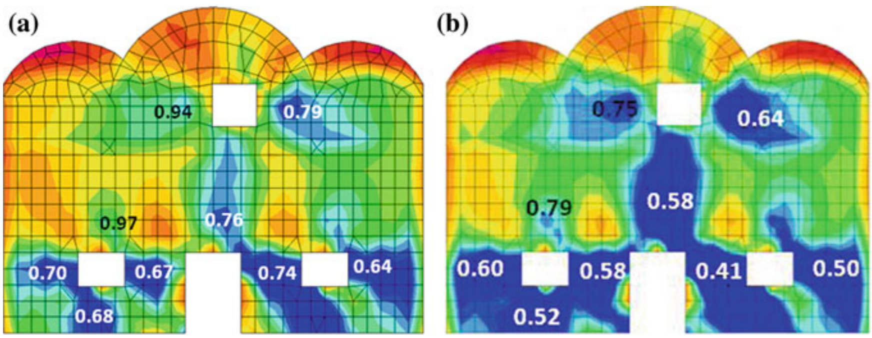

Fig. 17 Max in-plane shear stress strength/demand ratio **Rτ** internal transverse wall—load combination 0.9G+1.4(+Ey). **a** Non-deformable foundation. **b** Deformable foundation

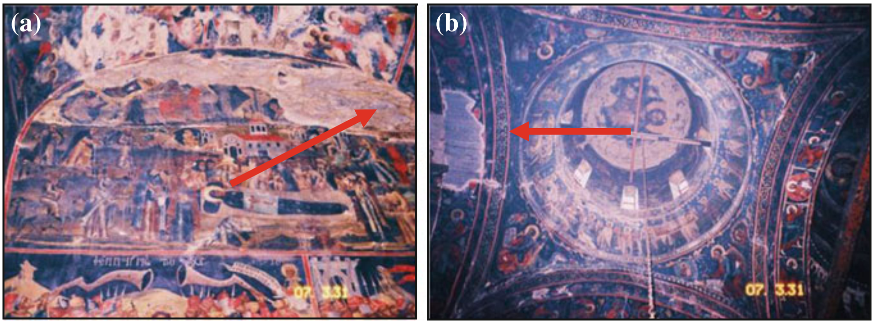

Fig. 18 Damage of the internal transverse wall and the adjacent arch. **a** Internal transverse wall. **b** Adjacent arch

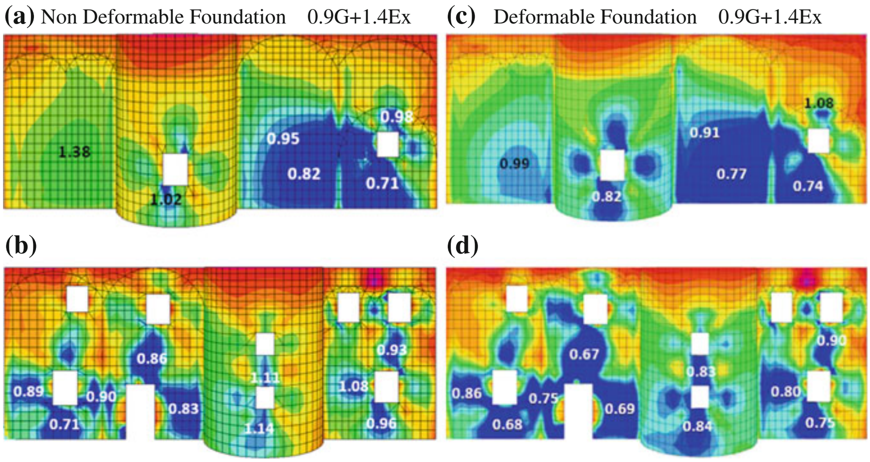

Fig. 19 Ratio values of $\mathbf{R}_\tau$ in-plane shear strength/shear demand. **a** North peripheral longitudinal wall. **b** South peripheral longitudinal wall. **c** North peripheral longitudinal wall. **d** South peripheral longitudinal wall

Fig. 20 Damage of the peripheral masonry walls

Figure 17 depicts the **Rτ** ratio values of the in-plane shear strength/shear demand for the load combination 0.9G+1.4Ey. The structural element that these ratio values belonged to is the internal transverse wall which separates the main church from the women's quarters situated at the West portion of the church. This wall (Fig. 18a) as well as the internal faces of all peripheral walls, vaults (Fig. 15b), arches (Figs. 15c and 18b) and domes (Fig. 15a) are decorated with very valuable frescos which bear signs of extensive damage.

Damage is also predicted by the numerical analysis results, as can be seen from the strength/demand **Rτ** ratio values that are well below 1, in many locations of the peripheral walls (Fig. 19a–d). The deformability of the foundation leads the **Rτ** ratio to attain values smaller than for the case of the non-deformable foundation, a

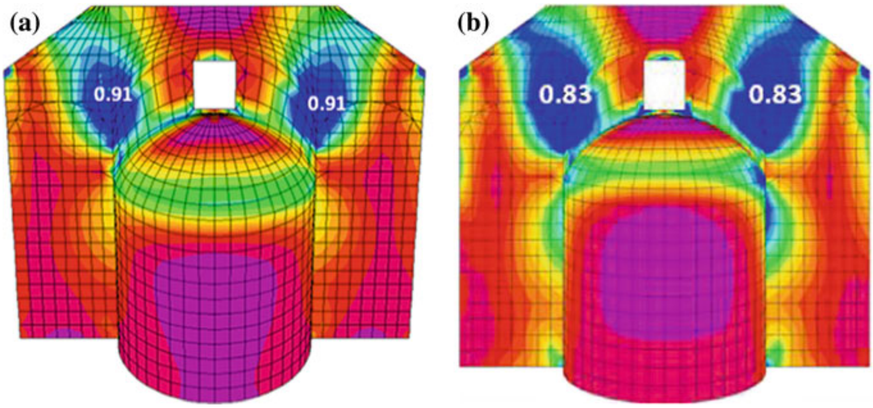

Fig. 21 East peripheral longitudinal wall, 0.9G+1.4Ex, ratio values of $\mathbf{R_M}$ out-of-plane $\boldsymbol{\sigma_{11}}$ normal strength/demand (*top face*). **a** Non-deformable-foundation. **b** Deformable foundation

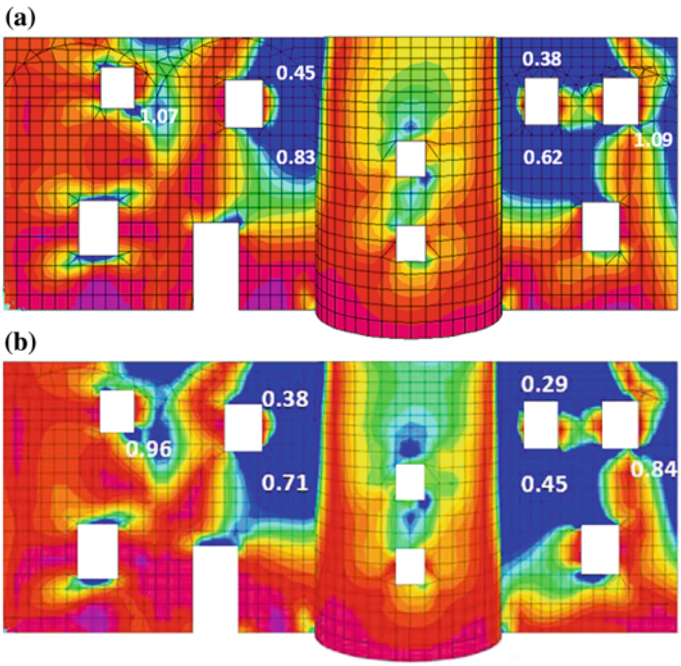

Fig. 22 Ratio values of $\mathbf{R_M}$ out-of-plane $\boldsymbol{\sigma_{11}}$ normal strength/demand (*top face*). **a** Non-deformable foundation South peripheral wall, 0.9G+1.4Ey. **b** Deformable foundation South peripheral wall, 0.9G+1.4Ey

fact that shows the detrimental effect of the flexibility of the foundation for this church.

The deformability of the foundation has similar effect for all peripheral walls. This can be seen either by studying the variation of the $\mathbf{R_\tau}$ values (in-plane shear strength/demand ratio, Fig. 19a–d) or the $\mathbf{R_M}$ values (out-of-plane tensile strength/demand ratio, Figs. 21 and 22). Such structural damage is visible from outside of this church at the lower parts of all the peripheral walls.

4 Damage of the "Church of Profitis Ilias at Siatista—Kozani"

This church is also a Post-Byzantine three nave Basilica built in 1701 A.D. on the top of a hill in the town of Siatista of the prefecture of Kozani. The superstructure includes a wooden roof without the vaulting system of the churches described in Sects. 2 and 3. The horizontal dimensions of this church are 23.25 m in length and 16.60 m in width. The top of the roof lies at 7.1 m from the floor level of the interior of this church. The naves are formed by 4-column colonnades (Fig. 23a, b) built

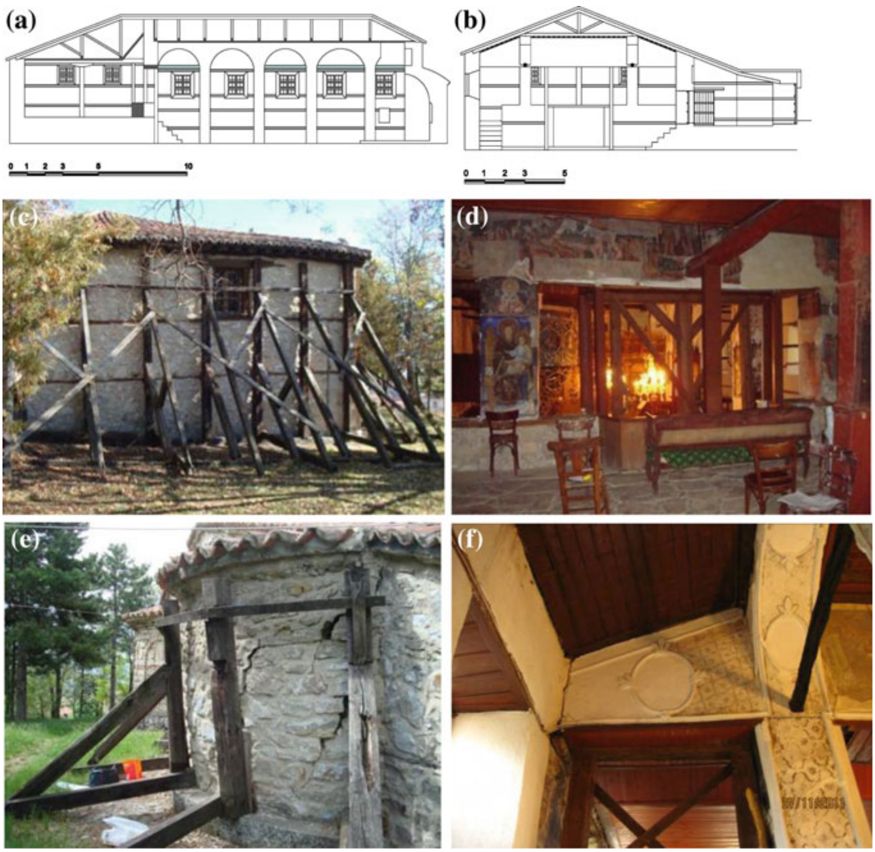

Fig. 23 The church of Profitis Ilias at Siatista—Kozani and observed damage. **a** Longitudinal cross-section. **b** Transverse cross-section. **c** Wooden shoring of South longitudinal wall. **d** Wooden shoring of mid-transverse wall. **e** Extensive cracking of the apse at the East wall. **f** Extensive cracking at the joint of the South longitudinal wall with the mid-transverse wall with its wooden shoring

with stone masonry. The lower part of the key of each arch of these colonnades lies at 5.25 m from the floor level of the interior of this church. All the exterior walls are made of stone masonry. Apart from the main church a narthex was built at the North side at a later stage. Due to the slope of the hill, this North part rises at a lower height from the ground level. The West part of the church is allocated to the women quarters which are separated from the rest of the interior by a mid-transverse wall (Fig. 23d). The South longitudinal wall is supported from the exterior by temporary wooden shoring, as shown in Fig. 23c. This was installed after the Kozani-1995 earthquake sequence [1] as an external support. Additional wooden supports were also placed in the interior of this church at the mid-span of the women quarters. According to past records, the structural system of this church has shown signs of distress from soil settlement sometime before the occurrence of this particular earthquake sequence. These records do not give information of any countermeasures being taken in the past prior to the occurrence of this earthquake. The main structural damage due to this earthquake sequence is as follows. Inclination of the South longitudinal wall outwards, accompanied with extensive cracking where this wall joins the East and West exterior masonry walls and the mid-transverse wall (Fig. 23f). Extensive cracking of the arches of the internal colonnades and the East wall apses was also observed (Fig. 23e). Recently, almost 18 years since the occurrence of this earthquake damage, a number of counter measures have been implemented, which are discussed in Sect. 5.

The current numerical investigation of this church includes the following:

- Simulation of the behaviour assuming non-deformable foundation.
- Simulation of the behaviour assuming deformable foundation level, by introducing at this level elastic springs with properties reflecting the actual soil deformability. This was found from in situ sampling of soil which consist of clay in its upper layers. In order to quantify the stiffness of these soil layers use was made of the data from three bore-holes drilled at the vicinity of the church at a depth up to 15 m.

All the numerical simulations assumed elastic behaviour with a relatively low values of the modulus of elasticity for the stone masonry equal to E = 1660 MPa. The thickness of the masonry walls varied from 0.75 to 1.0 m. The system of the wooden roof was modeled together with all the wooden elements that connect the longitudinal and transverse walls with the interior colonnades and the mid-transverse wall. Figure 24a–d depict the influence of the soil deformability on the displacement response due to the gravitational forces. The vertical as well as the horizontal displacement response is amplified due to this soil deformability.

A small number of mortar specimens were taken from this church. Some basic properties of these mortar samples are listed in Table 2. Moreover, the natural stone used in the masonry walls is a type of slate with a compressive strength equal to 24 MPa, as found from the literature survey. Table 3 lists the assumed mechanical characteristics for the stone masonry in terms of Young's modulus and Poisson's ratio as well as compressive and tensile strength values. These values were based on

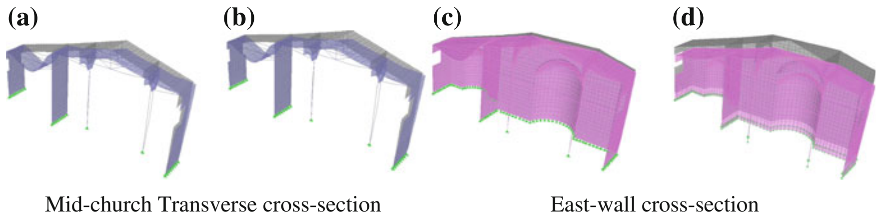

Fig. 24 Deformations for gravitational forces (Non-deformable/deformable foundation). **a** Non-deformable soil MaxUz = 1.2 mm, Ux = 0.2 mm. **b** Deformable soil Max Uz = 12 mm, Ux = 2 mm. **c** Non-deformable soil MaxUz = 0.8 mm, Ux = 0.2 mm. **d** Deformable soil Max Uz = 11.6 mm, Ux = 1.9 mm

Table 2 Characteristics of mortar samples taken from the church

Mortar sample code name	Absorption (%)	Specific gravity (KN/m^3)	Porous count (%)
K1	5.312	22.51	11.95
K2	0.51	27.22	13.89

Table 3 Assumed mechanical characteristics of the stone masonry

	Young's modulus (N/mm^2)	Poisson's ratio	Compressive strength (N/mm^2)	Tensile Strength normal/parallel bed-joint (N/mm^2)	Initial shear strength f_{vko} (N/mm^2)
Limit values	1660	0.2	1.0	0.10/0.25	0.10

data found in the literature and not in any direct measurements. From the comparison of the limit strength values of Table 3 with those of Table 1 it can be easily concluded that the stone masonry of this church (Profitis Ilias of Siatista) is much weaker than that of the church of Agia Triada at Vithos.

The same Mohr-Coulomb failure envelope, defined by Eq. 1 in Sect. 3, was also adopted here for the in-plane shear limit state of the stone masonry.

As was done before, the strength over demand ratios values at the most critical locations of the masonry walls were found by comparing the strength values, listed in Table 3, with the corresponding demand values, as they were obtained from the numerical simulation. With **Rσ** or with **Rτ** are the ratio values of the in-plane tensile or shear strength over the corresponding demand whereas $\mathbf{R_M}$ is the ratio value of the out-of-plane tensile strength over the corresponding demand. As stated before, ratio values smaller than 1.0 indicate that a limit state condition is reached thus predicting structural damage.

Rσ ratio values of in-plane strength/demand, applying the limit tensile strength scenario either normal to bed-joint ($\mathbf{F_{22}}$) or parallel to bed-joint ($\mathbf{F_{11}}$), are depicted in Fig. 25a–d for the masonry arches of the internal colonnades. The demands in these figures were obtained for the load combination G+0.3Q. As can be seen in these figures, the **Rσ** ratio values are smaller for the deformable than the non-deformable foundation, which demonstrates the detrimental effect of the foundation deformability for this church even only for the gravitational forces.

For the load combination 1.3G+1.5Q, that dictates the design for the gravitational forces under current code provisions, the above ratio values will become even smaller, which indicates that the colonnades can not withstand the maximum gravitational forces. This is verified by the observed damage for these structural elements at their current state, being supported since the earthquake event of 1995 by temporary wooden shoring (see Fig. 23c–f). The numerical simulation was also repeated for either load combinations 0.9G+1.4Ex or 0.9G+1.4Ey. Initially the seismic loads were considered as static forces Ex or Ey generated at the existing masses by a constant acceleration. The value of this constant acceleration was such that the resulting base shear attained approximately the same value that was found

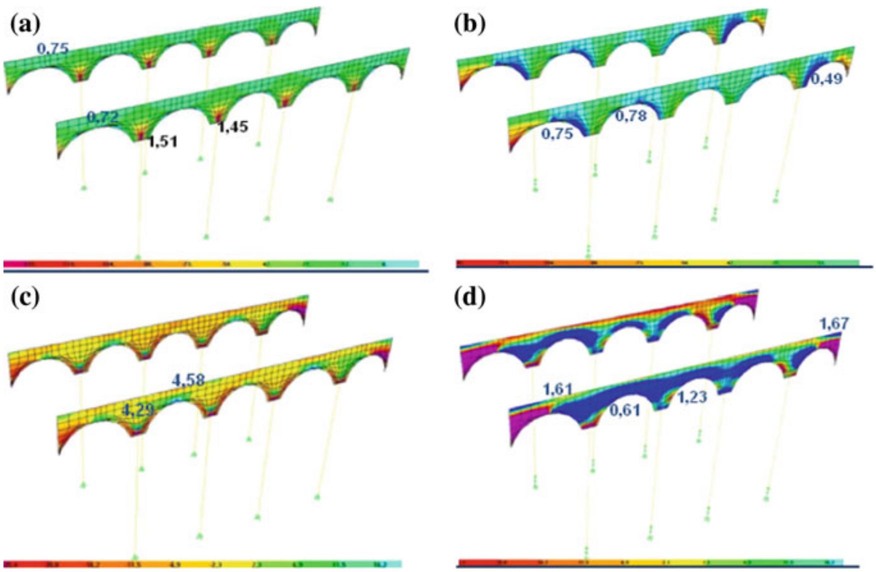

Fig. 25 Load combination G+0.3Q, $\mathbf{R}_\sigma$ ratio of in-plane strength/demand, North and South internal colonnades. **a** Non-deformable soil, ratio of $\mathbf{F}_{22}$ (KN/m) normal to bed joint. **b** Deformable soil ratio $\mathbf{F}_{22}$ (KN/m) normal to bed joint. **c** Non-deformable soil, ratio $\mathbf{F}_{11}$ (KN/m) parallel to bed joint. **d** Deformable soil, ratio $\mathbf{F}_{11}$ (KN/m) parallel to bed joint

when the earthquake actions were considered through a dynamic spectral analysis. In Fig. 26a, b the $\mathbf{R}_\mathbf{M}$ ratio out-of-plane strength/demand ($\boldsymbol{\sigma}_{11}$) are depicted.

The numerical simulation was repeated to include the seismic actions in the form of dynamic spectral analysis utilising the design spectrum derived by applying the provisions of the current Greek Seismic code for seismic zone I, soil category B and importance factor 1.3 [10].

This dynamic spectral analysis was based on sufficient number of eigen-modes capable of mobilising sums of modal mass larger than 65 % of the total mass of the structure. Figure 27a–f depict the most significant translational x-x and y-y eigen-modes together with their corresponding eigen-period and modal mass ratio values. This is done for both the non-deformable as well as the deformable foundation. As was also discussed before, the modal analysis results demonstrate one of the effects of the deformable foundation which is the lengthening of the eigen-periods of the most significant translational modes.

Several attempts have been made in the past to measure the dynamic characteristics (eigen-modes and eigen-frequencies) of cultural heritage structures through ambient vibration measurements in an effort to calibrate the numerical model parameters [12–17]. Because the structures examined here are quite stiff and in some cases quite complex it is difficult to practically utilize such a methodology. Alternatively, Low-intensity man made excitations can be also employed to

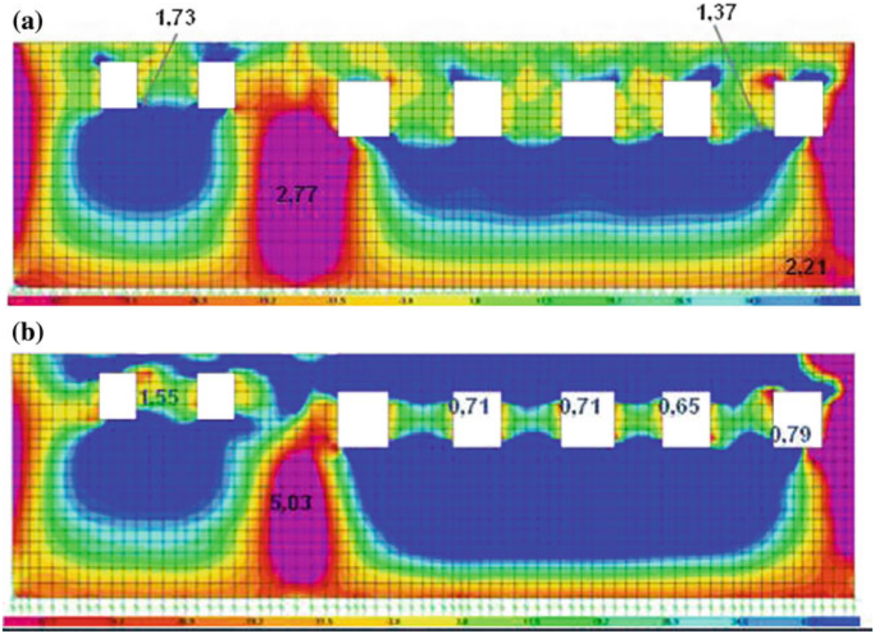

Fig. 26 0.9G+1.4E_y. $\mathbf{R_M}$ Ratio out-of-plane strength/demand $\boldsymbol{\sigma_{11}}$ outer-face. **a** Non-deformable soil. **b** Deformable soil

provide in situ measurements that can also be used to calibrate numerical models including influences arising from the soil-foundation interaction [18].

From the comparison of the demands, obtained from the numerical simulation, with the limit strength values adopted for the stone masonry of this church (Table 3) it can be concluded that the deformability of the foundation results in strength/demand ratio values ($\mathbf{R\tau}$, $\mathbf{R\sigma}$, $\mathbf{R_M}$) smaller than the corresponding ratio values for the non-deformable foundation. Such an evaluation has been performed for the most vulnerable structural elements of this church; that is the internal colonnades, the South peripheral wall and the East peripheral wall with the apses (Figs. 28, 29 and 30). Potential damage is predicted in this way when these strength/demand ratios attain values that are well below 1. These predictions are depicted in a summary form in Figs. 28, 29 and 30 through the values of ratios $\mathbf{R\tau}$ in-plane shear behaviour (green colour) $\mathbf{R\sigma}$ in-plane tensile behaviour (blue colour) $\mathbf{R_M}$ out-of-plane tensile behaviour (orange colour). In almost all structural elements the out-of-plane tensile behaviour results in strength/demand ratios ($\mathbf{R_M}$) with values well below 1. The smallest $\mathbf{R_M}$ ratio value appears to be located at the South longitudinal wall and is equal to 0.15. The average value of this $\mathbf{R_M}$ ratio obtained by averaging the corresponding values at six (6) different locations well spread over the entire length of this wall is equal to 0.245; this indicates that the demand for this wall in out-of-plane flexure exceeds four times the corresponding capacity. It is not surprising that this wall has visible signs of out-of-plane permanent displacements and

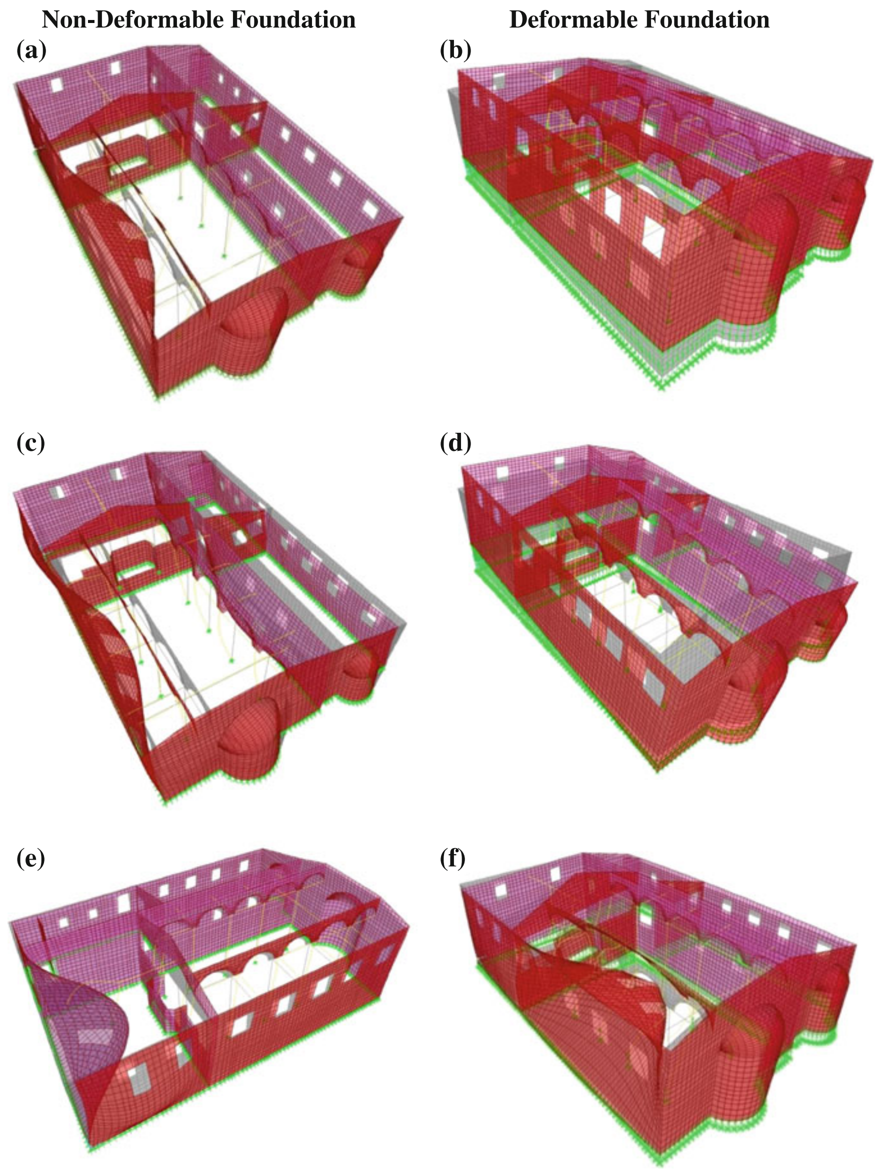

Fig. 27 The most significant eigen-modes for the non-deformable and the deformable foundation together with the values of the corresponding eogen-frequencies and modal mass participation ratios. **a** 1st y-y. Ty = 0.1179 s, Uy = 28.366 %. **b** 1st y-y. Ty = 0.212 s, Uy = 24.707 %. **c** 2nd y-y. Ty = 0.0937 s, Uy = 35.82 %. **d** 2nd x-x. Tx = 0.2007 s, Ux = 12.867 %. **e** 3rd x-x. Tx = 0.0917 s, Ux = 20.535 %. **f** 3rd y-y. Ty = 0.114 s, Uy = 10.236 %

Fig. 28 South peripheral wall. Regions with small values of the strength/demand $\mathbf{R_M}$ out-of-plane tensile behaviour (*orange color*), $\mathbf{R_\sigma}$ in-plane tensile behaviour (*blue color*)

Fig. 29 South internal colonnade. Regions with small values of the strength/demand $\mathbf{R_M}$ out-of-plane tensile behaviour (*orange color*), $\mathbf{R_\tau}$ in-plane shear behaviour (*green color*), $\mathbf{R_\sigma}$ in-plane tensile behaviour (*blue color*)

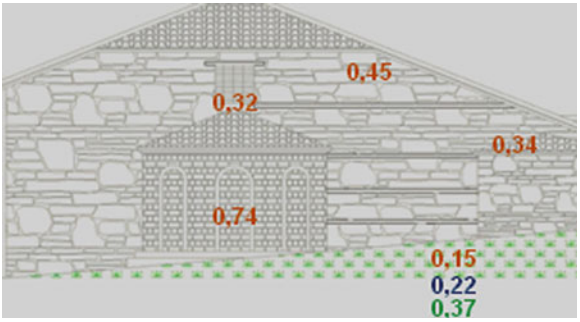

Fig. 30 East peripheral wall. regions with small values of the strength/demand $\mathbf{R_M}$ out-of-plane tensile behaviour (*orange color*), $\mathbf{R_\tau}$ in-plane shear behaviour (*green color*), $\mathbf{R_\sigma}$ in-plane tensile behaviour (*blue color*)

damage that is in agreement to the distress predicted by this approach. Such an evaluation procedure can also explain, up to a point, the development of the existing current state of structural damage. By all previous discussion the validity of this simplified methodology was portrayed. Consequently, it can then be extended for evaluating the effectiveness of potential retrofitting schemes. In order for such retrofitting schemes to be effective the resulting strength/demand ratios (**Rτ**, **Rσ**, **R_M**) should attain values larger than the corresponding values prior to retrofitting and, if possible, larger than 1.

5 Retrofitting—Experimental Investigation

The retrofitting of heritage structures is in general a difficult task as it cannot employ traditional retrofitting techniques that have been developed for reinforced concrete structures [19–21]; these can be termed as strong interventions that usually do not respect either the principle of compatibility of the old materials with the new materials or that of reversibility of the employed intervention scheme sometime in the future so that it can be replaced with a more efficient retrofitting scheme. The commonly applied retrofitting schemes usually mobilize the following:

- The upgrading of the strengths of the existing masonry. This is usually done with compatible mortars that can be injected with low pressure and fill the cavities of the stone masonry. This is further investigated by an experimental sequence that is presented in summary below.
- The strengthening of the wooden roof elements and their connection to the masonry.
- The replacement of the wooden ties and the addition of new visible metal ties.
- Strengthening of the foundation with various forms of external or internal encasement schemes. This has been proposed for the case of the church of Virgin Mary at Dilofo, presented in Sect. 2.
- Temporary or semi-temporary external shoring employing wooden, metal or reinforced concrete parts.
- Employing more advanced retrofitting methods, such as base isolation; Such a retrofitting schemes, although desirable because of their favourable effect, are usually faced with significant construction difficulties [22–26].

Semi-permanent shoring must be designed and constructed respecting the principle of reversibility as well as combined with the rest of the reversible techniques mentioned above. Such a retrofitting scheme is currently being investigated for Agios Dimitrios at Palatitsia Imathias, a 16th century three-nave Basilica; it is 27.10 m long on its South side and 22.15 m long on its North side with an average width 12.625 m. The height from the ground level to the top of the roof is 6.75 m (Fig. 31).

The studied retrofitting scheme consists of a system of semi-temporary shoring of the longitudinal peripheral walls together with the upgrading of the wooden roof, the replacement of the internal wooden ties together with the addition of new metal ties as well as mortar injections for all stone masonry. The performance of such a retrofitting scheme was investigated numerically by a full dynamic analysis (Fig. 32) employing the methodology described in all previous sections.

Fig. 31 The church of Agios Dimitrios at Palatitsia

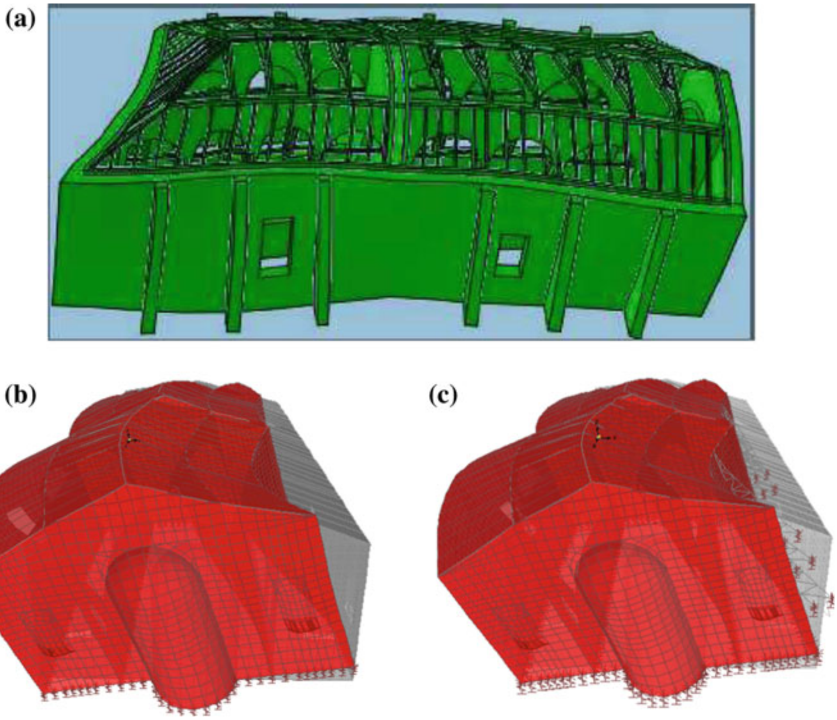

Fig. 32 Eigen-modes and eigen frequencies of Agios Demetrios at Palatitsia. **a** Retrofitted with seimi-permanent shoring. 2nd x-x translational eigen-mode. Tx = 0.2013 s, Ux = 38.5 %. **b** Present condition, deformable foundation, main transversal y-y eigen mode, T_y = 0.326 s Uy = 61.62 %. **c** Retrofitted with seimi-permanent shoring. Deformable foundation, main transversal y-y eigen mode, T_y = 0.263 s Uy = 68.17 %

The retrofitting scheme examined here takes a variety of alternative forms. The numerical results so far provide sufficient evidence that such a retrofitting scheme can be quite effective in upgrading the performance of the various stone masonry structural elements in such a way that their strength/demands ratio values **Rτ** in-plane shear, **Rσ** in-plane tension, and $\mathbf{R_M}$ out-of-plane tensile flexure, described before, obtain values larger than the corresponding values for its current state before any intervention. As already mentioned, the objective is for these strength/demands ratios to reach values larger than 1, ideally for all critical locations, thus signifying acceptable performance. The out-of-plane $\boldsymbol{\sigma_{22}}$ demands in the present condition (Fig. 33a) include large areas in the vicinity of the window openings with considerable tensile stress concentration exceeding the strength values, thus indicating potential structural damage regions. The introduction of the semi-permanent shoring resulted in a considerable decrease of these out-of-plane $\boldsymbol{\sigma_{22}}$ demands (Fig. 33b). This decrease in the demands combined with a considerable increase in the strength that is expected to be achieved from injecting the stone masonry with compatible mortar, will result in strength/demands ratios values (**Rτ** in-plane shear, **Rσ** in-plane tension, and $\mathbf{R_M}$ out-of-plane tensile flexure) larger than 1, thus demonstrating the effectiveness of the retrofitting scheme.

Retrofitting of heritage structures, like the churches that are presented in this study, becomes even more difficult when the stress field of the various structural

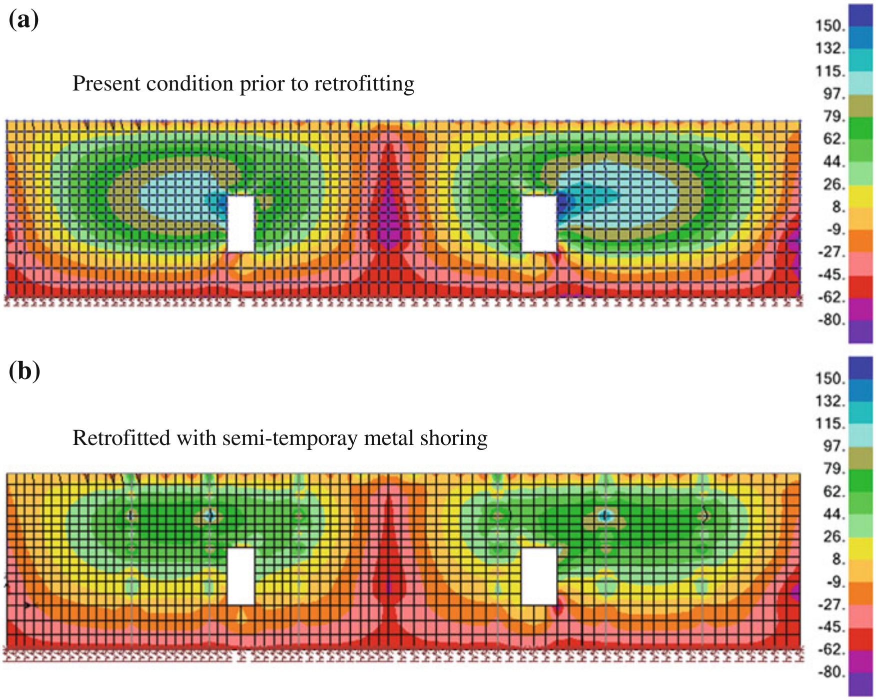

Fig. 33 Effect of retrofitting scheme in lowering the out-of-plane $\boldsymbol{\sigma_{22}}$ flexural demand. **a** South longitudinal wall, G+0.30Q+Ey deformable foundation, $\boldsymbol{\sigma_{22}}$ (kN/m^2, Kpa) normal stress bottom face. **b** South longitudinal wall, G+0.30Q+Ey deformable foundation, $\boldsymbol{\sigma_{22}}$ (kN/m^2, Kpa) normal stress bottom face

Fig. 34 Partial collapse of East part of the Virgin Mary at Dilofo (May 2014)

elements is influenced from uneven foundation settlements like the cases that were investigated here [27–30]. Most of the relatively mild counter-measures that were mentioned before, such as injections with compatible mortar re-pointing of the mortar joints, strengthening of the roof or introduction of metal ties or chords in various locations, are not sufficient to counteract the detrimental effect of uneven foundation settlements. This latter effect is further intensified by the dynamic progress of such foundation settlement with time unless effective countermeasures are applied. External wooden shoring can be effective provided that the transfer of forces from the damaged structure to the shoring is ensured and that the foundation of the external shoring is properly designed to withstand these forces without deformations that can render the transfer of forces ineffective. Usually, temporary shoring that is left in situ for long periods gradually becomes ineffective. Moreover, water erosion can speed up such deformations for both the foundation settlement as well as the deformations of the temporary shoring.

The temporary wooden shoring, constructed internally as well as externally, was partly employed in the cases of the church of Virgin Mary at Dilofo and Profitis Ilias at Siatista (see Figs. 2c and 23c). In the case of the church of Virgin Mary at Dilofo the ineffectiveness of the temporary shoring combined with the failure of an R/C surface beam, constructed externally at the bottom of the mainly damaged masonry walls at the East part of this church, exacerbated the damage and resulted in the partial collapse of most of this East part (Fig. 34).

5.1 Shear Capacity of Stone Masonry—Summary of Experimental Testing

A number of stone masonry specimens were built at the laboratory using lime mortar and natural stones. The lime mortar had such a composition as to be representative of old relatively weak mortars commonly used in the past. A series of such samples were tested accompanied by constant compression with variable shear as shown in Fig. 35b. This was designed in an effort to record the shear force at a

(a)

Mohr Coulomb failure criterion fv = fvo + 0.45 σ
fvo = 0.12 Mpa

	Normal Stress σ (Mpa)	Predicted fv = fvo + 0.45 σ (Mpa)	Measured value fv (Mpa)	Ratio Measured fv / Predicted fv
Sample 1	0.53	0.359	0.396	1.103
Sample 2	0.61	0.395	0.41	1.038
Sample 3	0.46	0.327	0.305	0.933
Sample 4α	0.30	0.255	0.20	0.784
Sample 4β	0.54	0.363	0.375	1.033

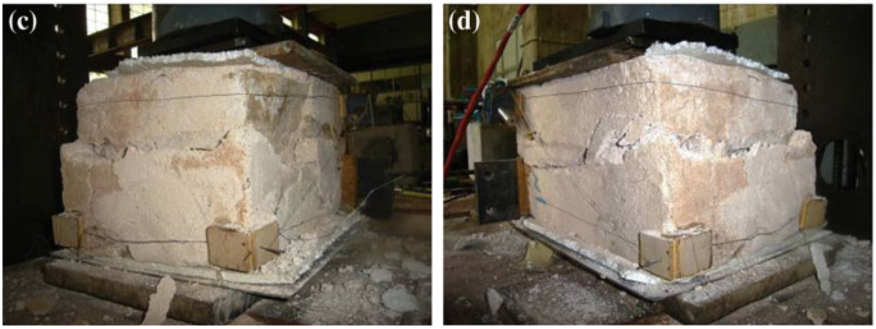

Fig. 35 Experimental investigation of the shear capacity of stone masonry. **a** Verification of the Mohr-Coulomb criterion. **b** Experimental set-up. **c** Sliding failure. **d** Sliding failure

limit state which represented the failure of the mortar bed-joint as is depicted in Fig. 35c, d. Based on these experimental results the Mohr-Coulomb criterion, used in this study, was quantified as shown in Fig. 35a.

6 Conclusions

- The eigen-periods, eigen-modes, and the deformation patterns to horizontal earthquake actions of the examined churches predicted numerically demonstrate certain behavioral characteristics that are of importance. They develop much larger displacements at the top of their longitudinal peripheral walls in a direction normal to the plane of these walls than at a direction parallel to that plane. Moreover, the presence of apses exercises a significant out-of-plane stiffening effect. The presence of stone masonry vaults increases the stiffening effect at the top of the peripheral wall level; however, such a stone masonry vaulting system also adds considerable masses at a high level that generate seismic actions of large amplitude.
- The numerical stress results together with assumed strength values for the various masonry elements of the examined churches predict that the most vulnerable regions to be damaged are near the door and window openings for the

in-plane behaviour. These regions together with the regions near the foundation appear to be the most vulnerable in out-of-plane bending, particularly for the longitudinal masonry walls. These regions, that are shown to be vulnerable to damage, are in reasonably good agreement, in a qualitative sense, with actual observed damage, despite the fact that the numerical simulation is based on elastic analysis assumptions. The employed limit state criteria of strength/demands ratio values, $\mathbf{R\tau}$ in-plane shear, $\mathbf{R\sigma}$ in-plane tensile, and $\mathbf{R_M}$ out-of-plane tensile behaviour lead to successful predictions of actual distress of the peripheral walls. When the superstructure consists of vaults and domes large seismic forces are generated that lead to areas of stress concentration at the bases of the domes and vaults and at the keys of the arches. Further investigation is needed to establish appropriate limit-state criteria for these stone masonry elements.

- The foundation deformability was also investigated introducing linear deformable springs at the foundation level. The results of such a numerical approximation combined with the followed methodology of limit state criteria of strength/demands ratio values, $\mathbf{R\tau}$ in-plane shear, $\mathbf{R\sigma}$ in-plane tensile, and $\mathbf{R_M}$ out-of-plane tensile behaviour demonstrated in all the examined cases that the foundation deformability, when combined with the gravitational forces and seismic actions, leads to $\mathbf{R\tau}$, $\mathbf{R\sigma}$, and $\mathbf{R_M}$ strength/demands ratio values that are considerably smaller than for the case of non-deformable foundation thus verifying the detrimental effect of the foundation deformability for all the examined cases.
- A retrofitting scheme that combines mortar grouting, wooden and metal ties, external semi-temporary shoring of the longitudinal walls together with foundation encasement is being currently investigated. The numerical results so far provide sufficient evidence that such a retrofitting scheme can be quite effective in upgrading the performance of the various stone masonry elements. This can be deduced from the numerical results whereby the $\mathbf{R\tau}$, $\mathbf{R\sigma}$, and $\mathbf{R_M}$ strength/demands ratio of the retrofitted structure attain values larger than the corresponding values for the structure in its current state before any intervention. The objective of the current study is for these strength/demands ratios to reach values larger than 1, ideally for all critical locations, thus signifying acceptable performance and demonstrating the effectiveness of the retrofitting scheme.
- An experimental sequence is also in progress that tries to quantify combined shear and compression limit-state criteria for stone masonry specimens that represent parts of the stone masonry walls prior to any intervention with mortar grout.
- The effects of foundation deformability in the form of permanent foundation settlement exhibit a dynamic progress with time unless effective countermeasures are applied that are properly designed and constructed. Retrofitting schemes for cultural heritage like the Christian churches presented here demonstrated the ineffectiveness of temporary counter measures.

References

1. Manos GC (2011) Consequences on the urban environment in Greece related to the recent intense earthquake activity. Int J Civ Eng Archit 5(12):1065–1090 (Serial No. 49)
2. Manos GC, Soulis V, Diagouma A (2008) Numerical investigation of the behaviour of the church of Agia Triada, Drakotrypa, Greece. J Adv Eng Softw 39:284–300
3. Manos GC, Soulis VJ, Felekidou O (2008) The dynamic and earthquake behaviour of greek Post-Byzantine Churches. 14WCEE, Beijing
4. Manos GC, Soulis VJ, Felekidou O, Koutsianou A, Lipiridou P (2009) The dynamic and earthquake response of Greek Byzantine and Post-Byzantine Basilicas. COMDYN 2009, Greece
5. Manos GC, Soulis V, Karamitsios N, Felekidou O (2009) Numerical simulation of the dynamic and earthquake behaviour of greek Post-Byzantine churches with and without base isolation. PROHITECH 2009, Rome, 21–24 June 2009
6. Manos GC, Soulis V, Felekidou O (2010) Numerical study of the dynamic and earth-quake behaviour of Byzantine and Post-Byzantine Basilicas. In: 8th international masonry conference, Dresden, Germany
7. Manos GC, Soulis V, Felekidou O, Matsou V (2010) A numerical investigation of the dynamic and earthquake behaviour of Byzantine and Post-Byzantine Basilicas. In: 9th U.S. national and 10th Canadian earthquake engineering conference, Toronto, Canada
8. Manos GC, Soulis V, Felekidou O, Matsou V (2010) A numerical investigation of the dynamic and earthquake behaviour of Byzantine and Post-Byzantine Basilicas. In: 3rd international workshop on conservation of heritage structures using FRM and SHM, Ottawa, Canada
9. Manos GC (2011) The bearing capacity of the assumption of Virgin Mary, a three-nave Basilica at Dilofo-Voio-Kozani and a retrofitting proposal. Technical report to the Greek ministry of culture (in Greek)
10. Provisions of Greek Seismic Code (2000) Organization of earthquake planning and protection of Greece OASP, Dec. 1999 published by OASP. Revisions of seismic zonation introduced in 2003, Government Gazzete, Δ17α /115/9/ΦN275, 1154, Athens, 12 Aug 2003
11. European Committee for Standardization, Euro code 6 (2005) Design of masonry structures. Part 1-1: General rules for building. Rules for reinforced and un-reinforced masonry. EN 1996-1-1
12. Verstrynge E, van Gement D, Schueremans L, Ignoul S (2010) Nitoring, assessing and strengthening historical masonry structures: case studies. CSHM-3, Canada, pp 321–330
13. Galino N, Gentile C, Saisi A (2009) Operational modal testing and analysis: an effective tool for the assessment of masonry towers. STREMAH-2009, Tallin, pp 487–498
14. Maeda T, Sugiura Y, Hirai T (2005) Vibration characteristics of the Bayon temple main tower, Angkor, Cambodia. STREMAH-2005, Malta, pp 255–264
15. Abruzzese D et al (2009) Dynamic investigations on medieval masonry towers: vibration measurements and structural identification. PROHITECH 09, pp 807–813. ISBN 978-0-415-55803-7
16. Casarin F, Valluzzi MR, da Porto F, Modena C (2008) Structural monitoring for the evaluation of the dynamic response of historical monuments. In: International RILEM conference on site assessment of concrete, masonry and timber structures, Italy, pp 787–796
17. Florio G, Formisano A, Landolfo R (2014) Seismic response and intervention strategy on the visitazione church in Poggio Picenze (AQ). In: Proceedings of the 2nd international conference on protection of historical constructions, pp 507–513. ISBN 978-975-518-361-9
18. Manos GC, Pitilakis KD, Sextos AG, Kourtides V, Soulis V, Thauampteh J (2014) Field experiments for monitoring the dynamic soil-structure-foundation response of model structures at a test site. J Struct Eng Am Soc Civil Eng 1–11. doi:10.1061/(ASCE)ST.1943-541X.0001154. © 2014, ISSN 0733-9445/D4014012

19. Earthquake Engineering Retrofitting of Heritage Structures (2013) Design and evaluation of strengthening techniques. In: Syngellakis S (ed) Wessex Institute of Technology, UK. ISBN: 978-1-84564-754-4, eISBN: 978-1-84564-755-1
20. Manos GC, Papanaoum E (2009) Earthquake behaviour of a R/C building constructed in 1933 before and after its repair. STREMAH 2009, Tallin, 22–24 June 2009
21. Organization of Earthquake Planning and Protection of Greece (OASP) (2012) Guidelines for retrofitting in reinforced concrete buildings, government gazette, Δ17α/04/5/ΦΝ 429–1, 42, Athens, 20 Jan 2012
22. Manos GC, Soulis V, Felekidou O, Karamitsios N, Kotoulas L (2010) Numerical study of the dynamic and earthquake response of greek Post-Byzantine churches with or without base isolation. In: 3rd international workshop on conservation of heritage structures using FRM and SHM, Ottawa
23. Manos GC, Karamitsios N (2011) Numerical simulation of the dynamic and earthquake behaviour of Greek Post-Byzantine churches with and without base isolation. COMPDYN 2011, Corfu, 26–28 May 2011
24. Manos GC, Karamitsios N (2011) Study of the dynamic and earthquake response of greek Post-Byzantine churches with and without base isolation. EURODYN 2011, Leuven, 4–6 July 2011
25. Manos GC, Karamitsios N (2011) Earthquake numerical simulation of the dynamic and earthquake behaviour of greek Post-Byzantine churches with and without base isolation. STREMAH-2011, Italy
26. Manos GC, Karamitsios N, (2013) Numerical simulation of the dynamic and earthquake behaviour of Greek Post-Byzantine churches with and without base isolation. Earthquake engineering retrofitting of heritage structures, design and evaluation of strengthening techniques, In: Syngellakis S (ed) Wessex Institute of Technology, UK, pp 171–186. ISBN: 978-1-84564-754-4, eISBN: 978-1-84564-755-1
27. Manos GC, Soulis VJ, Karamitsios N (2012) The performance of Post-Byzantine churches during the kozani-1995 earthquake—numerical investigation of their dynamic and earthquake behaviour. 15WCEE, Portugal
28. Manos GC, Kotoulas L, Matsou V, Felekidou O (2013) Dynamic behaviour of Greek Post-Byzantine churches with foundation deformability and evaluation of their earthquake performance. In: 4th ECOMASS thematic conference on computational methods in structural dynamics and earthquake engineering, COMPDYN 2013, Kos Island
29. Manos GC, Kotoulas L, Matsou V (2013) Numerical investigation of the influence of earthquake forces and foundation settlement on the performance of Post-Byzantine churches, Stremah-2013, Southampton
30. Manos GC, Kotoulas L (2014) Earthquake performance of greek Post-Byzantine churches with foundation deformability. In: Proceedings of 2nd international conference on protection of historical constructions, pp 297–303. ISBN 978-975-518-361-9